VTT Technical Research Centre of Finland

Open and ducted propeller virtual mass and damping coefficients by URANS-method in straight and oblique flow

Martio, Jussi; Sánchez-Caja, Antonio; Siikonen, Timo

Published in:
Ocean Engineering

DOI:
10.1016/j.oceaneng.2016.11.068

Published: 01/01/2017

Document Version
Early version, also known as pre-print

Open and Ducted Propeller Virtual Mass and Damping Coefficients by URANS-Method in Straight and Oblique Flow

Martio J.[1], Sánchez-Caja, A. [1], Siikonen, T. [2]

[1] VTT Technical Research Center of Finland

[2] Aalto University, Espoo (Finland)

ABSTRACT

The virtual mass and damping coefficients of an open and ducted propeller are determined using URANS computations. Time-accurate simulations are carried out for an open propeller forced to harmonic motion in two separate directions, translational x_1- and rotational x_4-directions. The analysis produces the diagonal coefficients of the virtual mass m_{11}, m_{44} together with the diagonal damping terms c_{11}, c_{44}. The cross-terms m_{14}, m_{41} and c_{14}, c_{41} are also evaluated. A range of advance numbers is considered in the simulations. Several excitation frequencies and amplitudes are applied in order to determine the impact of viscosity on the vibrational coefficients. Oblique flow cases are also considered and the related virtual mass and damping coefficients are analyzed. The computed cases are compared to potential flow simulations and to published semi-empirical results. The average magnitudes of the coefficients correspond quite reasonably to those computed by the CFD method. However, the viscous effects are found to have a certain impact on some coefficients.

Keywords

URANS, added mass, propeller, CFD, damping coefficients, vibration

1 INTRODUCTION

The evaluation of the vibrational properties of a marine propeller is important for a successful design. It is well known that the presence of water around a propeller vibrating as a part of a shafting system changes the dynamic characteristics of the propeller. Generally, the hydrodynamic forces acting on a propeller include terms proportional to the acceleration (mass/inertia forces), to the velocity (damping force) and to the displacement (hydrostatic force).

Concerning the first term of the vibrational analysis, the so-called effective or virtual mass/inertia of a propeller in water consists of not only the actual mass of the submerged propeller but also the mass of fluid accelerated with the propeller which is termed added mass/inertia. The second term needs special consideration depending on whether the propeller is locked or rotating. In the former case due to flow separation caused by off-design inflow excitations a velocity-dependent drag term should be included in the problem and in the latter case according to potential flow theory, circulatory forces proportional to the square of the velocity will be present affecting significantly the vibrational analysis of some particular motions. The third term, the hydrostatic force, is time-independent for fully submerged propellers and consequently does not contribute to vibrations except for partially submerged propellers. A description of the added mass, inertia and damping matrices in the classical vibrational analysis can be found for example in Carlton (2007).

Usually, the vibrating characteristics of a propeller have been calculated within potential-flow theory either in the form of two-dimensional thin foil theory, lifting line theory, lifting surface theory or panel methods (see, for example, Parsons and Vorus, 1981; Vassilopoulos and Triantafyllou, 1981; Parsons et al. 1983; Takeuchi et al. 1983; Matusiak, 1986; Ghassemi, 2011; Gaschler and Abdel-Maksoud, 2014) or with semi-empirical formulae (Schwanecke, 1963; MacPherson et al., 2007).

The use of potential flow theory for non-lifting fully-submerged bodies leads to added mass terms constant in time and with no damping. The introduction of the Kutta condition is responsible for the presence of velocity-dependent terms. Recently, Hutchison et al. (2013) investigated the effect of a duct on a non-rotating propeller by comparing the propeller and duct individually with the bodies combined in a multi-body simulation. The numerical analysis was based on panel methods and conducted with the commercial DNV software HydroD, using its WADAM program.

In the context of RANS methods, the introduction of viscosity in the simulation results in time-dependent added mass and damping coefficients especially for separated and cavitating flows (Uhlman et al. 2001; Lie et al. 2010). Recently, a method for calculating the translational added mass of axisymmetric bodies using a RANS solver has been presented by Mishra et al. (2011). The method removes the effect of the computed drag forces in the calculation of added mass coefficient. However, in our opinion if we stick to the definition of added mass in the second paragraph of

this section, the presence of viscosity would modify the mass of fluid accelerated with the body and consequently methods like that will be valid to estimate a *potential-flow added mass* using a viscous solver, but not a *viscous added mass*.

Much attention has been paid in the literature to the computation of the added mass coefficients for circular cylinders in various regimes of viscous flow and oscillating wings. However, to our knowledge there is a gap concerning the computations of such coefficients by RANS methods for rotating propellers. The present paper shows computations of added mass and damping coefficients for coupled torsional-axial motion and illustrates their variation as a function of the excitation frequency and advance number of the propeller.

Recently, some results of viscous added mass and damping coefficients for an open propeller were anticipated in Martio et al. (2015). The results are analyzed in detail in this paper and compared with semi-empirical formulae by Parsons (1981) and Schwanecke (1963) using the exact propeller geometry. Comparisons are made also with potential flow computations by Hutchison et al. (2013). The virtual mass and damping of a propeller are evaluated in viscous flow using URANS solver FINFLO (Sánchez-Caja et al., 1999; Miettinen and Siikonen, 2015). The coefficients are determined for a range of advance numbers J = [0.2,…,1.2]. The exciting frequency is varied between 0.25 and 1.6 times the blade passing frequency. Two configurations are analyzed in the computations: a propeller working in straight and oblique open flow and the same propeller working inside the 19A duct of MARIN (Wageningen). The computations are made at model scale.

2 NUMERICAL METHOD

2.1 Governing equations

The Navier-Stokes momentum equation for incompressible flow can be written for a control volume Ω delimited by a boundary$\partial\Omega$ as follows,

$$\rho\frac{\partial}{\partial t}\int_{\Omega(t)}\vec{v}\,dV+\rho\int_{\partial\Omega(t)}\left(\vec{v}(\vec{n}\cdot\vec{v}-\vec{n}\cdot\vec{v}_b)\right)dS = -\int_{\partial\Omega(t)}\vec{n}p\,dS+\mu\int_{\partial\Omega(t)}\vec{n}\cdot\nabla\vec{v}dS \tag{1}$$

where ρ is the density,$\vec{v}$ is the flow velocity vector, $\vec{v}_b$ is the velocity vector on the boundaries, p is the pressure in the flow field , $\vec{n}$ is the vector normal to the boundary, dS the surface element and μ is the viscosity. The boundary $\partial\Omega(t)$ consists of a moving boundary attached to the surfaces of an oscillating body and an external and stationary boundary which may extend to infinity.

From Eq. (1) the virtual mass and damping coefficients can be derived as follows. If a propeller is moving in unidirectional motion and is simultaneously in harmonic motion, the instantaneous state vector is $[x_i, V_A+\dot{x}_i, \ddot{x}_i]$. The harmonic velocity t term $\dot{x}_i$ and the harmonic acceleration $\ddot{x}_i$ are defined as

$$\dot{x}_i = \dot{x}_{ia}\sin(\omega t)\,;\quad \ddot{x}_i = \dot{x}_{ia}\,\omega\cos(\omega t) \tag{2}$$

where $\dot{x}_{ia}$ is the velocity amplitude of the harmonic motion to a given direction x_i, i=1…6.

If the control volume Ω is large enough so that it includes the particles at the location when the propeller started rotating, the convection term at the left side of Eq. (1) vanishes in a global sense. Using the propeller's instantaneous velocity $V_A+\dot{x}_i$ Eq. (1) can be made non-dimensional as follows,

$$\rho\ddot{x}_i D^3\int_{\Omega}\vec{v}_0\,dV_0+\rho n(V_A+\dot{x}_i)D^3\frac{\partial}{\partial t_0}\int_{\Omega}\vec{v}_0 dV_0 = -D^2\int_{\partial\Omega(t)}\vec{n}p\,dS_0+\mu D^2\int_{\partial\Omega(t)}\vec{n}\cdot\nabla\vec{v}dS_0 \tag{3}$$

where $\vec{v}_0$ is the non-dimensiolized fluid velocity and t_0 a time made non-dimensional with the inverse of the propeller rotational speed n. A non-dimensional volume is defined as $V_0=\frac{V}{D^3}$ while the non-dimensional area can be expressed as $S_0=\frac{S}{D^2}$. Notice that since the term used for non-dimensionalization is time-dependent but not space-dependent, it can be transferred outside the integral.

Furthermore, the fluid velocity vector can be separated into three components by applying the Helmholtz decomposition:

$$\vec{v}=\vec{v}_\infty+\vec{v}_\phi+\vec{v}_\psi \tag{4}$$

where $\vec{v}_\infty$ is the uniform inflow velocity at infinity upstream, $\vec{v}_\phi$ is the velocity component of the perturbation potential and $\vec{v}_\psi$ is the velocity component due to viscous effects. The last term will be responsible for the viscous component of the added mass and the damping term.

The velocity $\vec{v}_\infty$ consists of the speed of advance V_A into the given direction x_i, where i=1…3 and of the harmonic velocity $\dot{x}_i$. Eq. (4) states that the viscous term $\vec{v}_\psi$contributes both to virtual mass and damping terms, whereas the potential flow term $\vec{v}_\phi$ has impact to the virtual mass component only.

The force components of Eq. (3) can be expressed as

$$\begin{aligned} T_{mi}\ddot{x}_i+T_{ci}\dot{x}_i+T_{0i}&=T(t)\\ Q_{mi}\ddot{x}_i+Q_{ci}\dot{x}_i+Q_{0i}&=Q(t)\end{aligned} \tag{5}$$

T_{mi} is the acceleration-related added mass term, T_{ci} is the damping term associated to the harmonic velocity

component and T_{0i} is the force component generated by the propeller average thrust related to the steady velocity V_A. All terms correspond to motions in the *i*-direction. Q_{mi}, Q_{ci} and Q_{0i} are the corresponding terms for the torque.

Eq. (3) can be approximated by the following linear semi-empirical fitting for translational oscillations in direction x_1,

$$\rho D^3 m_{11}\ddot{x}_1 + \rho n D^3 c_{11}\dot{x}_1 + \rho n^2 D^4 K_{T1} = T(t) \qquad (6)$$

The corresponding formulation for the rotational oscillations in direction x_4 is

$$\rho D^4 m_{44}\ddot{x}_4 + \rho n D^4 c_{44}\dot{x}_4 + \rho n^2 D^5 K_{Q4} = Q(t) \qquad (7)$$

The thrust and torque coefficients, the diagonal elements of the virtual mass matrix and the diagonal damping terms are defined as follows,

$$\begin{aligned} K_{T1} &= \frac{T_{04}}{\rho n^2 D^4};\ K_{Q4} = \frac{Q_{04}}{\rho n^2 D^5} \\ m_{11} &= \frac{T_{m1}}{\rho D^3};\ c_{11} = \frac{T_{c1}}{\rho n D^3} \\ m_{44} &= \frac{Q_{m4}}{\rho D^4};\ c_{44} = \frac{Q_{c4}}{\rho n D^4} \end{aligned} \qquad (8)$$

The cross-terms related to rotational motion are evaluated as follows,

$$\rho D^4 m_{14}\ddot{x}_4 + \rho n D^4 c_{14}\dot{x}_4 + \rho n^2 D^4 K_{T4} = T(t) \qquad (9)$$

where,

$$\begin{aligned} m_{41} &= \frac{Q_{m1}}{\rho D^4};\ c_{41} = \frac{Q_{c1}}{\rho n D^4} \\ m_{14} &= \frac{T_{m4}}{\rho D^4};\ c_{14} = \frac{T_{c4}}{\rho n D^4} \end{aligned} \qquad (10)$$

The coefficients are expressed by a set of selected dimensionless parameters describing the flow conditions. For example, in the direction x_1 the dimensionless parameters obtained from Eq. (3) are as follows,

$$\begin{aligned} J &= \frac{V_A}{nD};\quad Re_p = \frac{\rho \dot{x}_{1a} D}{\mu} \\ KC_p &= \frac{f_e}{n} \end{aligned} \qquad (11)$$

where n is the propeller rotational speed (rps). The advance number J is related to the average loading on the propeller, whereas the frequency parameter KC_p and the Reynolds number Re_p are associated to the harmonic flow components. In this paper, the evaluated force coefficients are parametrized by J and KC_p.

2.2 URANS solver FINFLO

The flow solution in FINFLO is based on the RANS equations solved by a pressure correction approach. The spatial discretization is carried out by a finite volume method. Second- and third-order upwind-biased (MUSCL) schemes are used for the discretization of the convection terms and a second-order central-difference scheme is utilized for the diffusion. The pressure gradient is centrally differenced and a Rhie-Chow type dissipation is applied to prevent a checkerboard pressure field (Miettinen and Siikonen, 2015).

A multigrid method is applied for the acceleration of convergence. Solutions on coarse grid levels are used as a starting point for the calculation in order to accelerate convergence. A detailed description of the numerical method including discretization of the governing equations, solution algorithm, boundary conditions, etc. are described by Sánchez-Caja et al. (1999) and by Miettinen and Siikonen (2015). Several turbulence models are implemented in FINFLO. In these calculations Chien's low Reynolds number k- turbulence model is used. Time-accurate calculations are started by using a quasi-steady solution as the initial guess. In the time-accurate calculations part of the grid is rotating at the propeller rotational speed and part of the grid is stationary. The sliding mesh technique is used to treat the interface between the rotating and the stationary part of the grid. The variables are interpolated on the sliding boundary using the solution in the neighboring blocks. FINFLO computational approach includes also the possibility to use the overlapping (Chimera) grid technique.

Table I. Geometrical data of the P1374 model propeller.

Propeller diameter	250.0 mm
Number of blades Z	4
Pitch/Diameter at r/R=0.7	1.1
Hub diameter	60.0 mm
Expanded area ratio	0.602
Expanded skew angle	23 deg

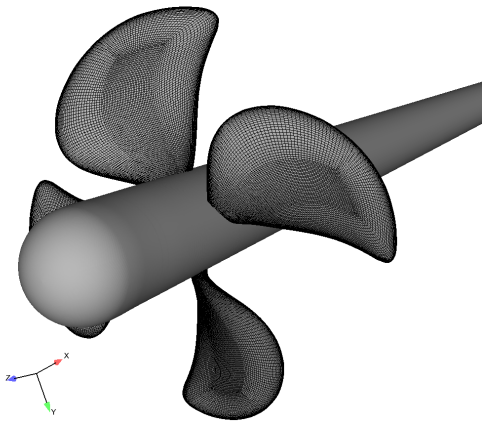

Figure 1a: RANS grid on the blades of propeller P1374.

3 STUDY CASES

3.1 The P1374 propeller

The P1374 propeller and related experimental data used in this research were provided by MARINTEK (Koushan, 2006). The main parameters of the propeller are shown in Table I. A perspective view of the propeller geometry with the grid on the blades is presented in Figure 1a, and the propeller-duct configuration is shown in Figure 1b. As it can be seen from the figures, the grid is very dense on the blades. It consists of 27 blocks with a total of 5.3 million cells for a blade passage.

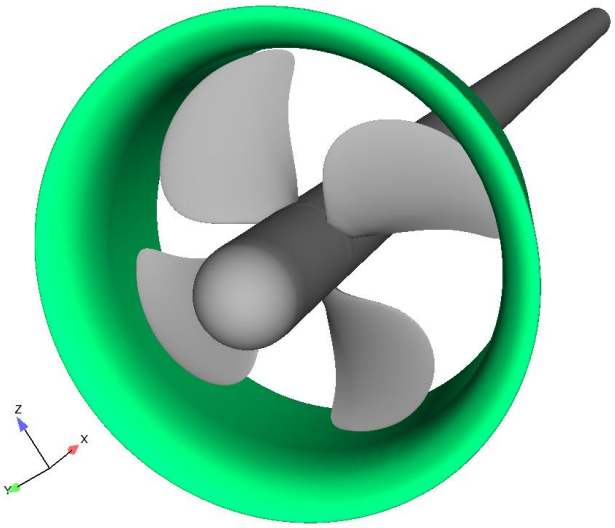

Figure 1b: View of propeller P1374 inside nozzle 19A.

3.2 Boundary conditions for harmonic oscillations

The computational grid covers a single-blade passage so that cyclic boundary conditions can be applied on the appropriate boundaries. On the blade surface, a non-slip boundary condition was used on the rotating blades (ROT), whereas on the nozzle surface a stationary non-slip boundary condition was utilized. In the external boundaries inlet and outlet boundary conditions on velocity and pressure, respectively were applied. The ROT-condition was modified to enforce oscillating motions in the x_1 and x_4-directions. The additional harmonic component on the grid and solid surfaces (ALE method) was:

$$\vec{v}_b = \vec{v}_{Ab} sin(\omega t) \tag{12}$$

which resulted in an instantaneous acceleration

$$\vec{a}_b = \vec{v}_{Ab} \omega cos(\omega t) \tag{13}$$

with $\vec{v}_{Ab}$ equal to $-x_{1a}\omega$ for the $\dot{x}_1$ term and $-x_{4a}\omega$ for the $\dot{x}_4$ term.

The parameters used in rotational oscillations are presented in Table II. They have been chosen to be meaningful from the standpoint of test measurements, even though some extreme cases have been also included. The case with excitation frequency f_e=9.0 Hz and amplitude x_{4a}=5.0 deg was evaluated for three advance numbers J=0.40, 0.60 and 0.80. The blade passing frequency was f=36.0 Hz in all cases corresponding the propeller rotational speed n=9.0 Hz. The physical time step applied in computations corresponds the rotational angle of one degree. The parameters used in the translational oscillations are shown in Table III.

Table II. Parameters for the rotational oscillations.

Case	Excitation frequency f_e [1/s]	Angle amplitude x_{4a} [deg]	Velocity amplitude $\dot{x}_{4a}$ [deg/s]	Advance number
1.1	9.0	5.0	282.7	0.40
1.2	9.0	5.0	282.7	0.60
1.3	9.0	1.0	56.5	0.80
1.4	22.5	1.0	141.4	0.80
1.5	40.5	1.0	254.5	0.80
1.6	9.0	5.0	282.7	0.80
1.7	22.5	5.0	706.9	0.80

Table III. Parameters for the translational oscillations.

Case	Excitation frequency f_e [1/s]	Displacement amplitude x_{1a} [m]	Velocity amplitude $\dot{x}_{1a}$ [m/s]	Advance number J
2.1	22.5	0.00043	0.0601	0.2
2.2	49.5	0.00009	0.0283	0.2
2.3	31.5	0.00032	0.0641	0.2
2.4	31.5	0.00046	0.0913	0.2
2.5	57.9	0.00016	0.0568	0.2
2.6	40.5	0.00037	0.0938	0.2
2.7	40.5	0.00041	0.1037	0.2
2.8	22.5	0.00032	0.0451	0.8
2.9	22.5	0.00043	0.0601	0.8
2.10	49.5	0.00009	0.0283	0.8
2.11	31.5	0.00046	0.0913	0.8
2.12	57.9	0.00016	0.0568	0.8
2.13	40.5	0.00037	0.0938	0.8
2.14	40.5	0.00041	0.1037	0.8
2.15	40.5	0.00049	0.1241	0.8
2.16	49.5	0.00009	0.0283	1.2
2.17	31.5	0.00046	0.0913	1.2

2.18	49.5	0.00026	0.0816	1.2
2.19	40.5	0.00049	0.1241	1.2

The computations of the ducted propeller were carried out for two rotational and for two translational harmonic motions. The oscillation parameters were x_{4a}=1.0 deg and 5.0 deg using f_e=22.5 Hz and x_{1a}=6.37 m/s with f_e=22.5 Hz and 23.9 m/s using f_e=40.5 Hz applied to the rotational motion x_4 and the translational motion x_1, respectively.

4 RESULTS

4.1 Open water characteristics

Figure 2 and Table IV show the open water performance coefficients (thrust coefficient, torque coefficient and efficiency) evaluated by FINFLO compared to the experimental values. The agreement is satisfactory except for large advance number, which is expected due to the larger uncertainty related to small thrust coefficients.

4.2 Open Propeller: Added inertia and damping

Rotational motion

In Figure 3, the total thrust T, the fluctuating pressure force component T_P and the harmonic viscous force term T_V are presented for case 1.7. The phase angle between the viscous force term and the other force components is approximately π. The magnitude of viscous component is small compared to the pressure term.

Computations of vibrational coefficients for cases 1.3 and 1.7 are presented in Figure 4. The forces of case 1.3 include minor non-linear elements, whereas those of case 1.7 present almost purely linear oscillations. Case 1.7 can be considered as an extreme situation, as the thrust and the torque both change sign during the simulations.

Table IV. Open water characteristics of P1374-propeller, open propeller case

J	Computed K_T	Exp K_T	K_T diff. to exp. %	Computed K_Q	Exp K_Q	K_Q diff. to exp. %
0.2	0.519	0.528	1.7 %	0.817	0.798	-2.4 %
0.4	0.423	0.431	1.9 %	0.703	0.687	-2.3 %
0.6	0.329	0.335	1.8 %	0.574	0.572	-0.3 %
0.8	0.229	0.241	5.0 %	0.439	0.452	2.9 %
1.0	0.131	0.140	6.4 %	0.319	0.311	-2.6 %

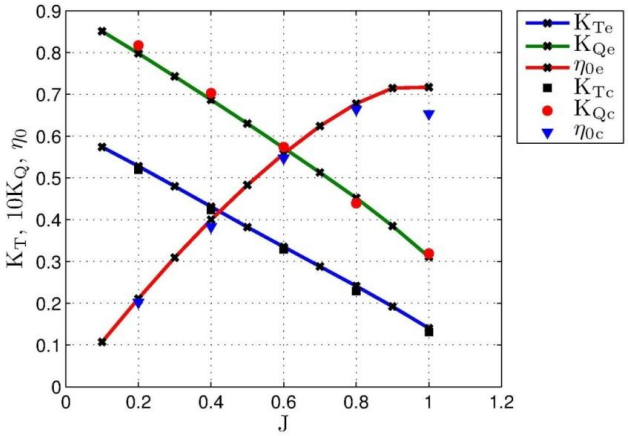

Figure 2. Propeller P1374 open water performance. The experimental values (sub-index *e*) are shown together with the computed (sub-index *c*) ones.

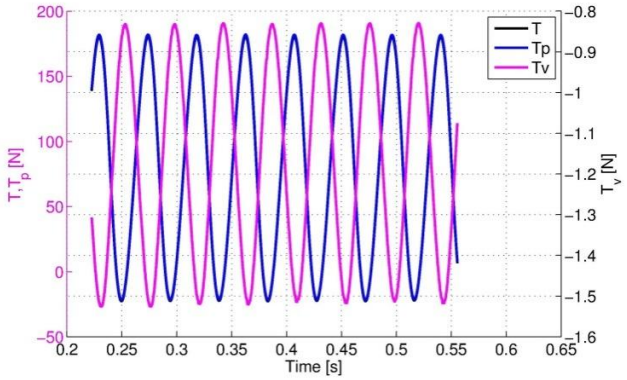

Figure 3. Computed force as a function of time for case 1.7. Total thrust force T, pressure component T_p and the viscous component T_v.

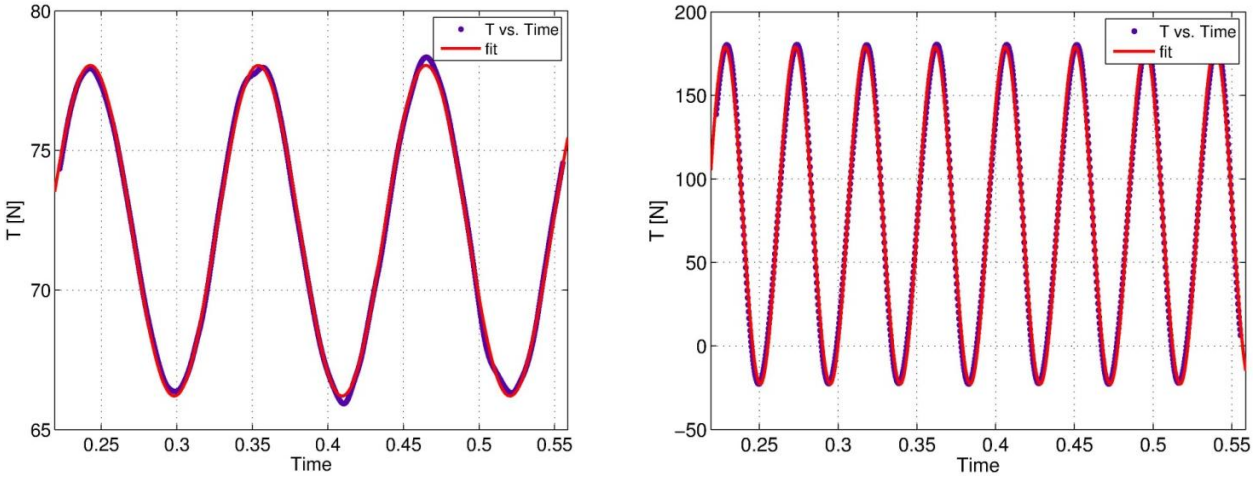

Figure 4. Computed forces as a function of time [s] for case 1.3 (left) and 1.7 (right). The red line represents the fitted function and the blue dots are the computed forces.

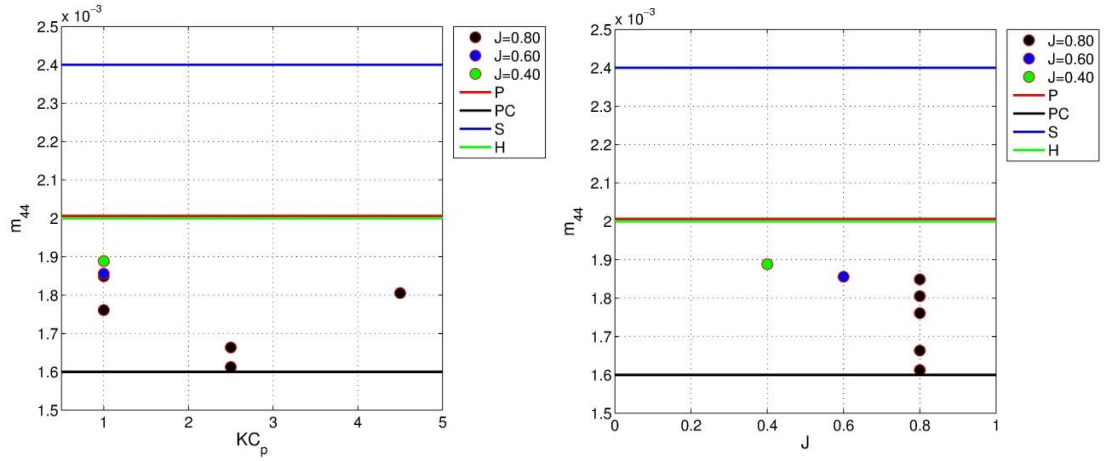

Figure 5a: Added mass coefficient m_{44} as a function of KC_p and of the advance number J. 'P' corresponds the method by Parsons (1981), 'PC' includes the lift surface correction by Parsons (1981), 'S' denotes the semi-empirical method by Schwanecke (1963) and 'H' stands for the potential flow computations by Hutchison (2013).

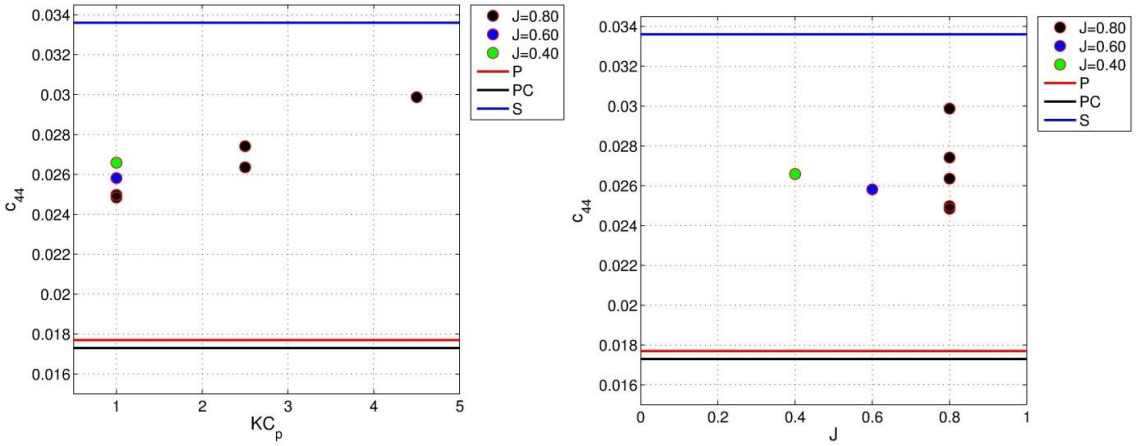

Figure 5b: Damping coefficient c_{44} as a function of KC_p and of the advance number J. 'P' corresponds the method by Parsons (1981), 'PC' includes the lift surface correction by Parsons (1981) and 'S' denotes the semi-empirical method by Schwanecke (1963).

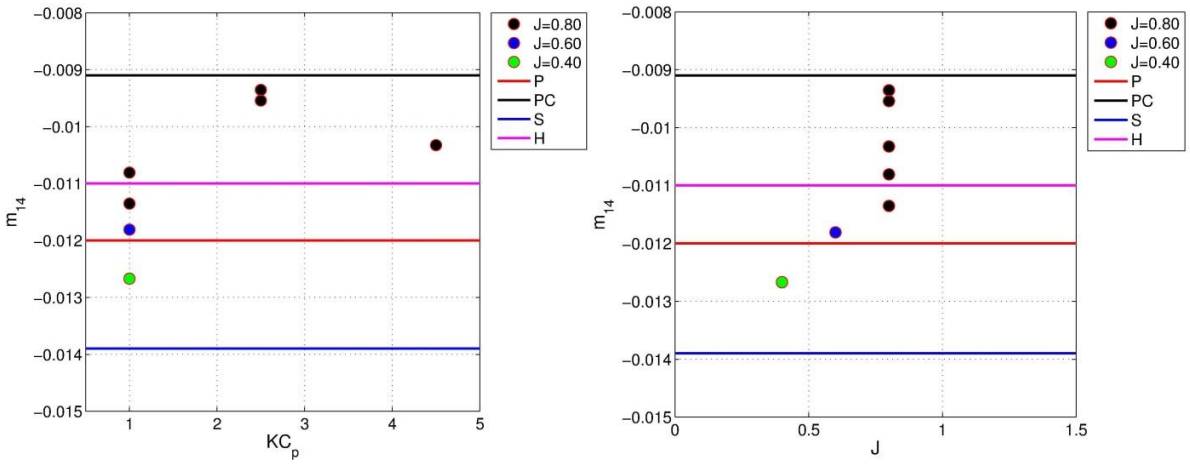

Figure 6a: Added mass coefficient m_{14} as a function of KC_p and of the advance number J. 'P' corresponds the method by Parsons (1981), 'PC' includes the lift surface correction by Parsons (1981), 'S' denotes the semi-empirical method by Schwanecke (1963) and 'H' stands for the potential flow computations by Hutchison (2013).

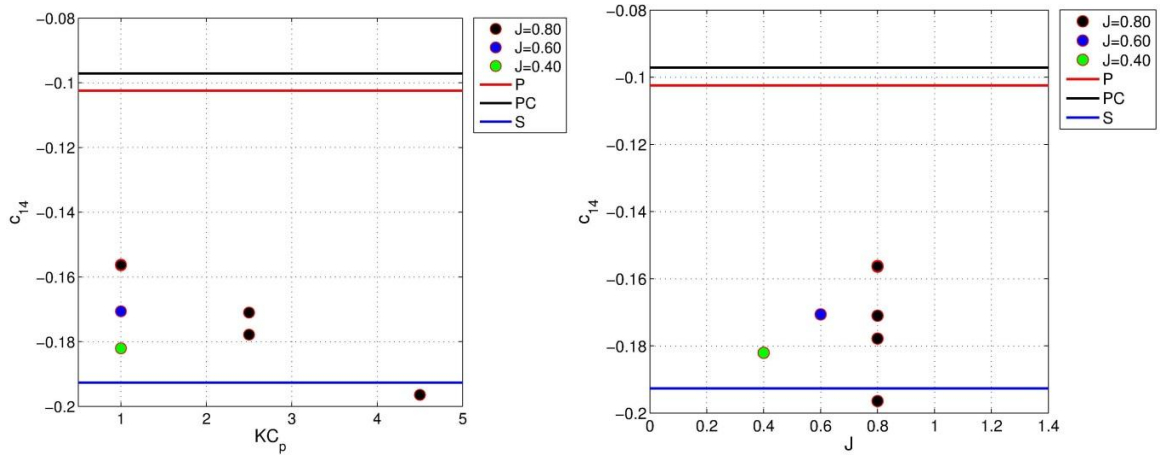

Figure 6b: Damping coefficient c_{14} as a function of KC_p and of the advance number J. 'P' corresponds the method by Parsons (1981), 'PC' includes the lift surface correction by Parsons (1981) and 'S' denotes the semi-empirical method by Schwanecke (1963).

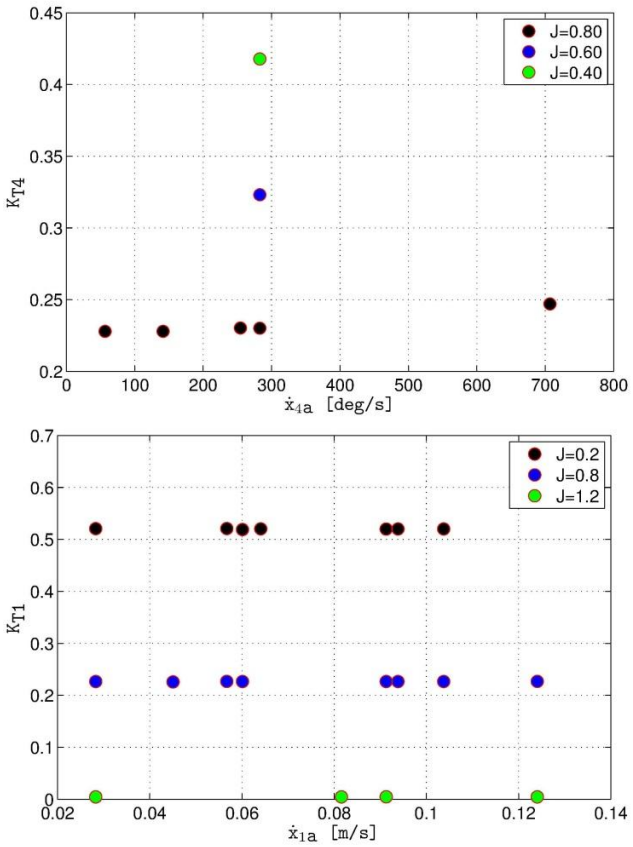

Figure 7. Thrust coefficients K_{Ti} as a function of amplitude $\dot{x}_{ia}$. The advance numbers are presented in different colors.

The force coefficients m_{44} and c_{44} together with the cross-terms m_{14} and c_{14} are presented in Figures 5 and 6 as a function of KC_p and advance number J. The damping coefficients c_{14} and c_{44} can be parametrized in terms of KC_p without large dispersion. The added inertia coefficients produce somewhat more scattering. In the J-domain the coefficients are subject to large dispersion. In the figures, different advance numbers for the same frequency are located in the same vertical line and viceversa (different frequencies for the same advance number).

In the figures, the results computed using the URANS-method are compared to estimates obtained with the semi-empirical methods by Schwanecke (1963) and Parsons (1981), and with a potential flow method (Hutchison, 2013). Generally, quite substantial variations can be observed between the specific methods. Schwanecke's method yields a m_{44} coefficient larger than other methods as shown in Figure 5a. The panel method results by Hutchison and the semi-empirical technique by Parsons generate similar m_{44} coefficients. The URANS coefficients are between Parsons' method estimates with and without lifting surface corrections. The lifting surface corrections have an effect similar to that described in Parsons' paper: they reduce the magnitude of coefficients. A similar comparison was carried out in Martio et al., (2015): the coefficients computed with the URANS method were compared to those obtained by Schwanecke's method. In the present paper, Schwanecke's semi-empirical coefficients were recalculated using the revised propeller geometry.

The magnitudes of c_{44} damping coefficients shown in Figure 5b diverge also rather substantially. The URANS coefficients are between the coefficients determined by semi-empirical methods (i.e. Parsons and Schwanecke).

A similar behavior can be seen for the m_{14} and c_{14} coefficients in Figure 6a and 6b. The panel method (Hutchison) produces quite similar estimates compared to the method by Parsons without lifting surface corrections, and the computed coefficients are again between the semi-empirical methods.

The K_{T1} and K_{T4} coefficients are shown as a function of the excitation amplitude in Figure 7. The oscillations produce only minor impacts on the average K_{T1} coefficient, of the order of 1% or less for cases 2.1-2.15. As the advance number is increased, the oscillations seem to reduce the K_{T1} as compared to the non-oscillating cases. Regarding the coefficient K_{T4}, the most extreme case 1.7 induces ~10 % larger average thrust than cases 1.3-1.6.

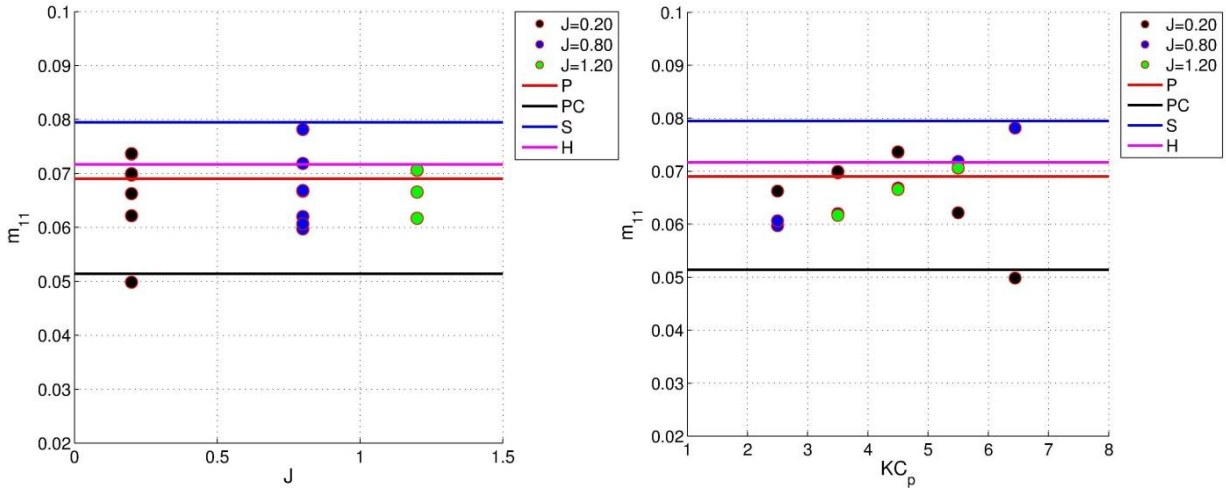

Figure 8a. Added mass m_{11} as a function of KC_p and of the advance number J. 'P' corresponds the method by Parsons (1981), 'PC' includes the lift surface correction by Parsons (1981), 'S' denotes the semi-empirical method by Schwanecke (1963) and 'H' stands for the potential flow computations by Hutchison (2013).

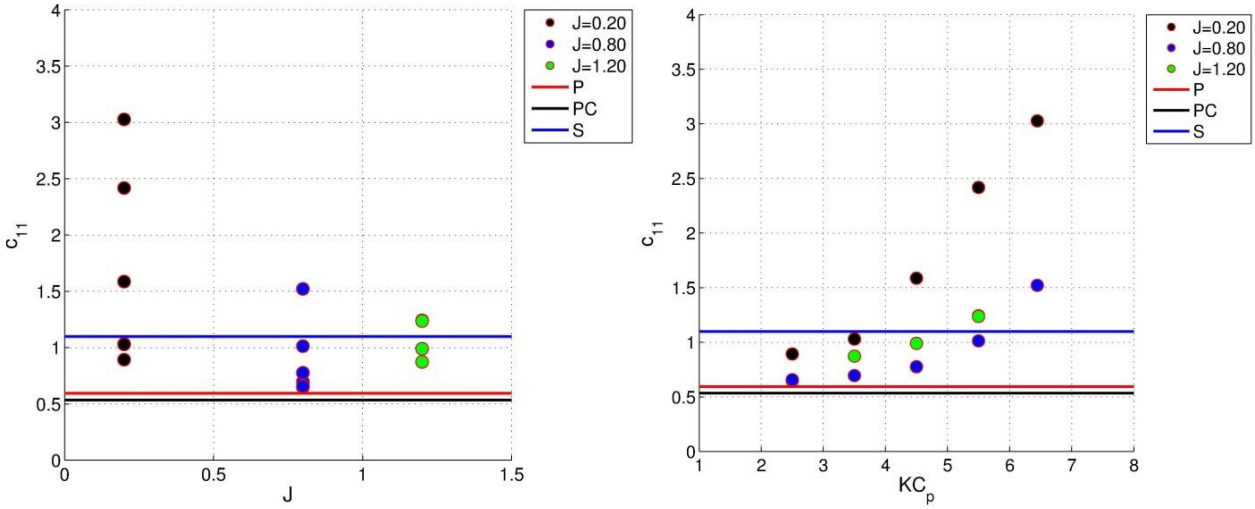

Figure 8b. Damping coefficient c_{11} as a function of KC_p and of the advance number J. 'P' corresponds the method by Parsons (1981), 'PC' includes the lift surface correction by Parsons (1981), 'S' denotes the semi-empirical method by Schwanecke (1963) and 'H' stands for the potential flow computations by Hutchison (2013).

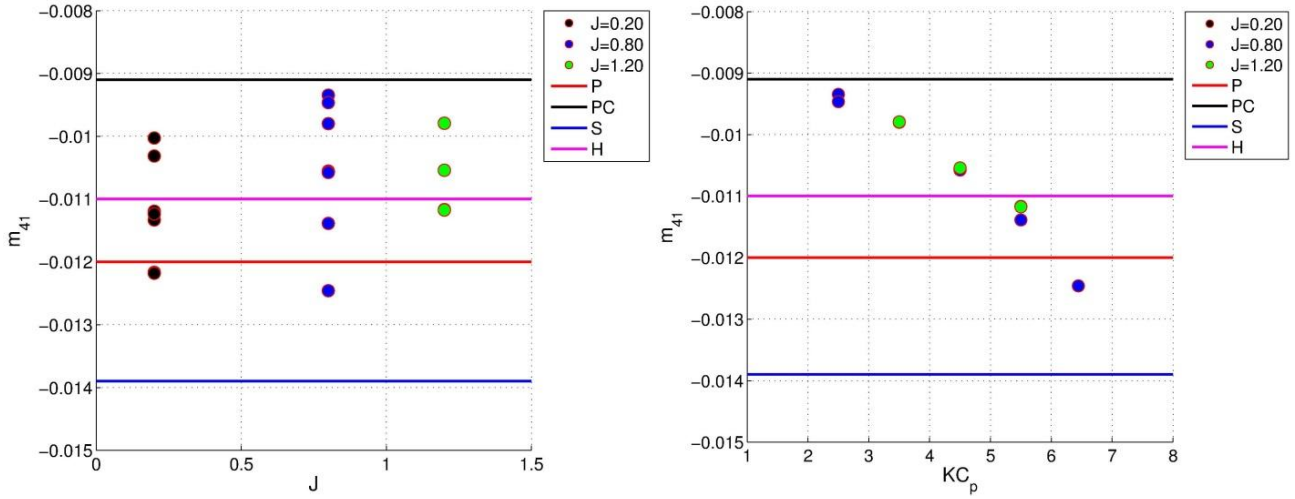

Figure 9a. Added mass coefficients m_{41} as a function of KC_p and of the advance number J. 'P' corresponds the method by [Parsons'PC' includes the lift surface correction by Parsons (1981), 'S' denotes the semi-empirical method by Schwanecke (1963) and 'H' stands for the potential flow computations by Hutchison (2013).

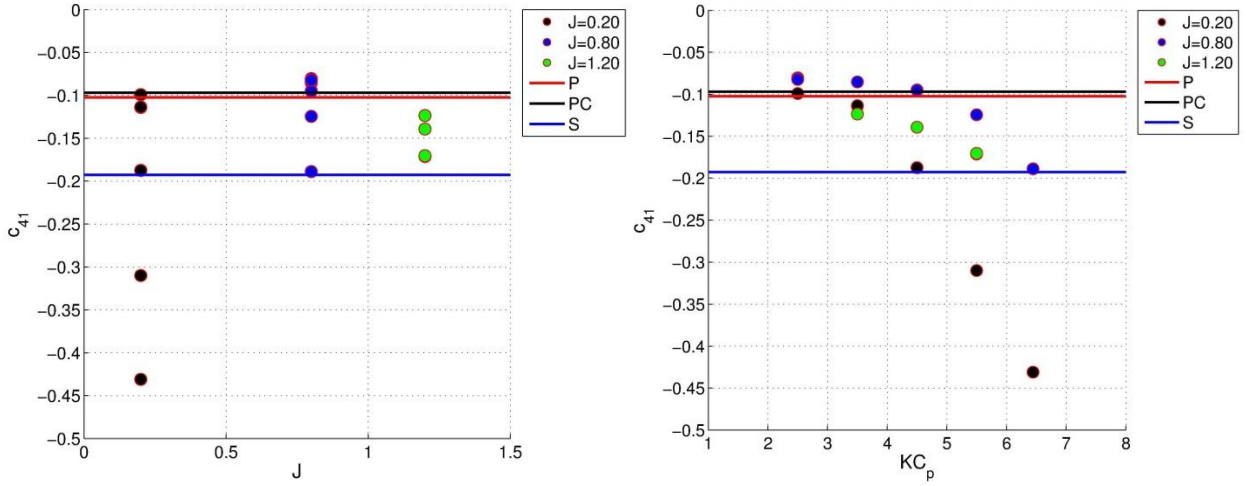

Figure 9b. Damping coefficient c_{41} as a function of KC_p and of the advance number J. 'P' corresponds the method by [Parsons'PC' includes the lift surface correction by Parsons (1981), 'S' denotes the semi-empirical method by Schwanecke (1963) and 'H' stands for the potential flow computations by Hutchison (2013).

Table V. The added inertia and damping force components in rotational harmonic motion x_4. The bold-italic font style denotes the ducted cases

x_{4a} [deg]	f_e/n	J	m_{44}	c_{44}	m_{14}	c_{14}	K_{T4}
1.0	2.5	0.8	0.00161	0.0264	-0.00935	-0.171	*0.228*
5.0	2.5	0.8	0.00166	0.0274	-0.00954	-0.178	0.247
1.0	***2.5***	***0.8***	***0.00161***	***0.0350***	***-0.00914***	***-0.218***	***0.184***
5.0	***2.5***	***0.8***	***0.00165***	***0.0376***	***-0.00944***	***-0.233***	***0.199***

Table VI. The virtual mass and damping force components in translational harmonic motion x_1. The bold-italic font style denotes the ducted cases.

$\dot{x}_{1a}$[m/s]	J	f_e/n	m11	c11	m14	c14	K_{T1}
6.37	0.8	2.5	0.0597	0.649	-0.00925	-0.0818	0.226
23.88	0.8	4.5	0.0668	0.776	-0.01063	-0.0958	0.227
6.37	***0.8***	***2.5***	***0.0692***	***1.112***	***-0.01065***	***-0.1534***	***0.184***
23.88	***0.8***	***4.5***	***0.0821***	***1.546***	***-0.01281***	***-0.2083***	***0.184***

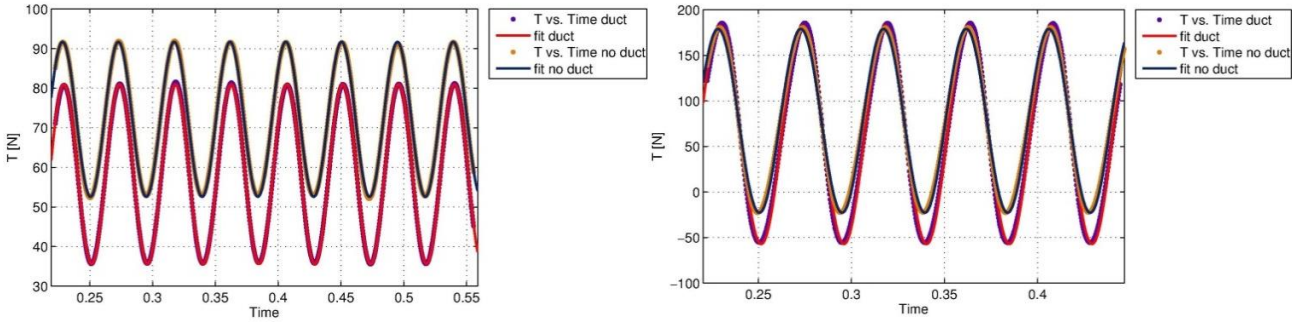

Figure 10. The evaluated forces as a function of time (s) for cases f_e=22.5 Hz, x_{4a}=1.0 deg (left) and f_e=22.5 Hz, x_{4a}=5.0 deg (right) at J=0.8 both for the ducted and the open propeller cases.

Translational motion

The time histories of the total thrust force T and of the viscous and pressure components are similar to the rotational motion case. They include some non-linearities in the viscous term, being again the magnitude of viscous component rather small compared to the pressure component. They are not presented here.

The harmonic coefficients m_{11}, c_{11}, m_{41} and c_{41} are shown in Figures 8-9 as a function of KC_p and J. The trends compared to the semi-empirical methods and potential flow computations are similar to those shown for the motion x_4 in Figures 5-6. The computed coefficients are generally between those determined by the methods by Parsons (1981) and Schwanecke (1963), although the computed damping coefficient c_{11} and c_{41} are larger in magnitude than semi-empirical coefficients especially at low advance numbers and for high frequency. At these conditions the viscous effects are more dominant.

Also the potential flow method (Hutchison, 2013) produces similar magnitudes of added mass coefficients as the URANS method, although it should be kept in mind that the potential flow evaluation was conducted with the locked propeller. According to MacPherson (2007) the relationship between the added mass coefficients for a rotating and a locked propeller can be expressed as follows:

$$C_{WER} = \frac{C_{WEL}}{2.09 - 1.51\left(\frac{P}{D}\right) + 0.62\left(\frac{P}{D}\right)^2} \quad (14)$$

where C_{WER} is the added mass for the rotating propeller and C_{WEL} is the added mass for the locked case. Applying Eq. (14) to the P1374 propeller, the magnitude of the added mass coefficient for the locked case should be 17 % larger than for the rotating case. If this is taken into account, the magnitude of added mass coefficient m_{11} by Hutchison should be reduced about that percentage from the level shown in Figure 8a.

4.3 Ducted propeller: added inertia and damping

The P1374 propeller inside nozzle 19a of MARIN has been analyzed under both rotational and translational harmonic oscillations. The characteristics of the ducted propeller were evaluated only for the advance number J=0.8. A rotational harmonic motion was applied only to the propeller, i.e. the nozzle was not subject to any oscillations. For the translational oscillations, surface velocities were enforced on the propeller surface and the RANS simulations were conducted in a time-accurate manner.

The magnitude of harmonic coefficients is presented in Table V for the rotational motion x_4 and in Table VI for the translational motion x_1. The thrust coefficients of the ducted

cases are clearly smaller than the open propeller cases due to the axial acceleration of the flow induced by the duct. Figure 10 shows the time histories of the computed forces both for the ducted and open propeller cases.

In Figures 11-12 the computed coefficients of the ducted cases are presented for comparison with the open propeller cases. The added mass coefficients computed by the potential flow method (Hutchison, 2013) are also shown for both the open propeller and ducted configurations. Generally, the duct seems to have only minor impact onto the virtual mass terms for the m_{44} and m_{14} coefficients. On the other hand, the nozzle seems to contribute more to the damping terms, i.e. the ducted cases produce larger c_{11}, c_{44} terms whereas the magnitude of cross-terms c_{41}, c_{14} is lower.

The potential flow method (Hutchison) predicts trends for the added mass coefficients m_{11}, m_{44} and m_{41} similar to the URANS-technique. In other words, the absolute magnitudes of coefficients m_{11} and m_{41} increase due to the presence of nozzle. The magnitudes of coefficients m_{44} and m_{14} related to rotational motion x_4 change only slightly between the open propeller and ducted propeller cases. The duct has an evident impact on the inflow velocity to the propeller, which seems to influence more noticeably the coefficients related to the translational motion x_1. The potential flow method (Hutchison, 2013) seems to estimate larger changes for the coefficient m_{14} than the URANS method. However, in this respect, it should be recalled that the potential flow method produces a symmetric added mass matrix, that is, m_{14}=m_{41} and that the potential flow analysis was made on a locked propeller contrary to the RANS simulation which was made on a rotating one.

In principle it seems surprising that there is (according to Table VI) almost no effect of the duct on the added mass of the propeller in rotational motion. On the contrary, the increase of the damping terms is more according to expectations. However, the added mass effect is not so surprising if we consider the potential flow part of the problem. Suppose a flat plate oscillating in the vertical direction (OY). The main parameter affecting the added mass is the length of the projection of the flat plate on the OX axis (i.e. the chord). Suppose that now the flat plate oscillates in the horizontal OX direction. The main parameter affecting the added mass is the length of the projection of the flat plate on the OY axis (i.e. zero). For a *rotating* propeller the effective inflow at the propeller tip is almost in the chordwise direction (close to the circumferential direction). The m_{44} related oscillations are in the circumferential direction and they do not change so much the effective angle of attack, which means that the effect is similar to OX oscillations of a flat plate at small angle of attack. For a non-rotating propeller especially at mid span the oscillating flow is not chordwise oriented and therefore a larger effect in m_{44} is expected. Additionally the m_{44} includes also a viscous part whose contribution is difficult to guess.

4.4 Oblique cases

The oblique flow cases were computed for 5, 10 and 20 degree flow angle. The vibrational coefficients are shown in Table VII including zero angle case 2.8.

The time histories of the thrust force are presented in Figure 13. The zero angle case produces the lowest average thrust, since the propeller is more loaded with the lower axial inflow of the oblique flow cases. The coefficients in Table VII indicate that the magnitudes of virtual masses m_{11} and m_{41} decrease whereas the damping is increased once an oblique flow angle is specified. However, there is no much influence between the 5, 10 and 15 deg cases.

5 CONCLUSIONS

Added mass and damping coefficients were computed by a URANS approach for the P1374 propeller in model scale. Harmonic motions were enforced at two degrees of freedom, i.e. in translational x_1- and rotational x_4-directions. The propeller was also analyzed both in oblique flow and in the presence of a duct.

The viscous flow simulation produces coefficients that are dependent from the excitation parameters, contrary to usual potential flow simulations where the coefficients are constant. The coefficients obtained from the URANS-simulation were compared to those obtained from the semi-empirical methods by Schwanecke (1963) and Parsons (1981) and to those obtained in Hutchison (2013) by a potential flow panel method. The dependency of the URANS coefficients with the excitation parameters was expressed in terms of appropriate non-dimensional numbers reflecting time-dependence like the KC_P parameter. The average magnitudes of the coefficients were reasonable as compared against the semi-empirical results, although the semi-empirical coefficients varied quite substantially depending on the specific method.

The magnitudes of the added mass coefficients were not much affected by the presence of the duct at the rotational motions, whereas the magnitudes of translational coefficients were increased. The comparison of URANS added mass coefficients to published potential-flow-based coefficients (Hutchison, 2013) revealed similar trends when passing from the open propeller to the ducted propeller configuration. The nozzle contributed also to the damping terms in such a way that the translational damping terms were increased together with the rotational damping coefficients.

In the oblique inflow computations, the presence of an incidence angle increased the magnitudes of translational damping coefficients relative to the straight flow cases. However, the magnitudes of translational virtual mass coefficients were reduced. Once the flow is non-

axisymmetric, the magnitude of the angle of incidence seems not to affect too much the coefficients.

ACKNOWLEDGMENTS

This research was funded by the EU MARTEC project HyDynPro. We are grateful to the research partners and funding institutions for their interest in this work. The authors are grateful to MARINTEK for providing the geometry and the test data of propeller P1374, and to Prof. Sverre Steen for his useful comments on the paper.

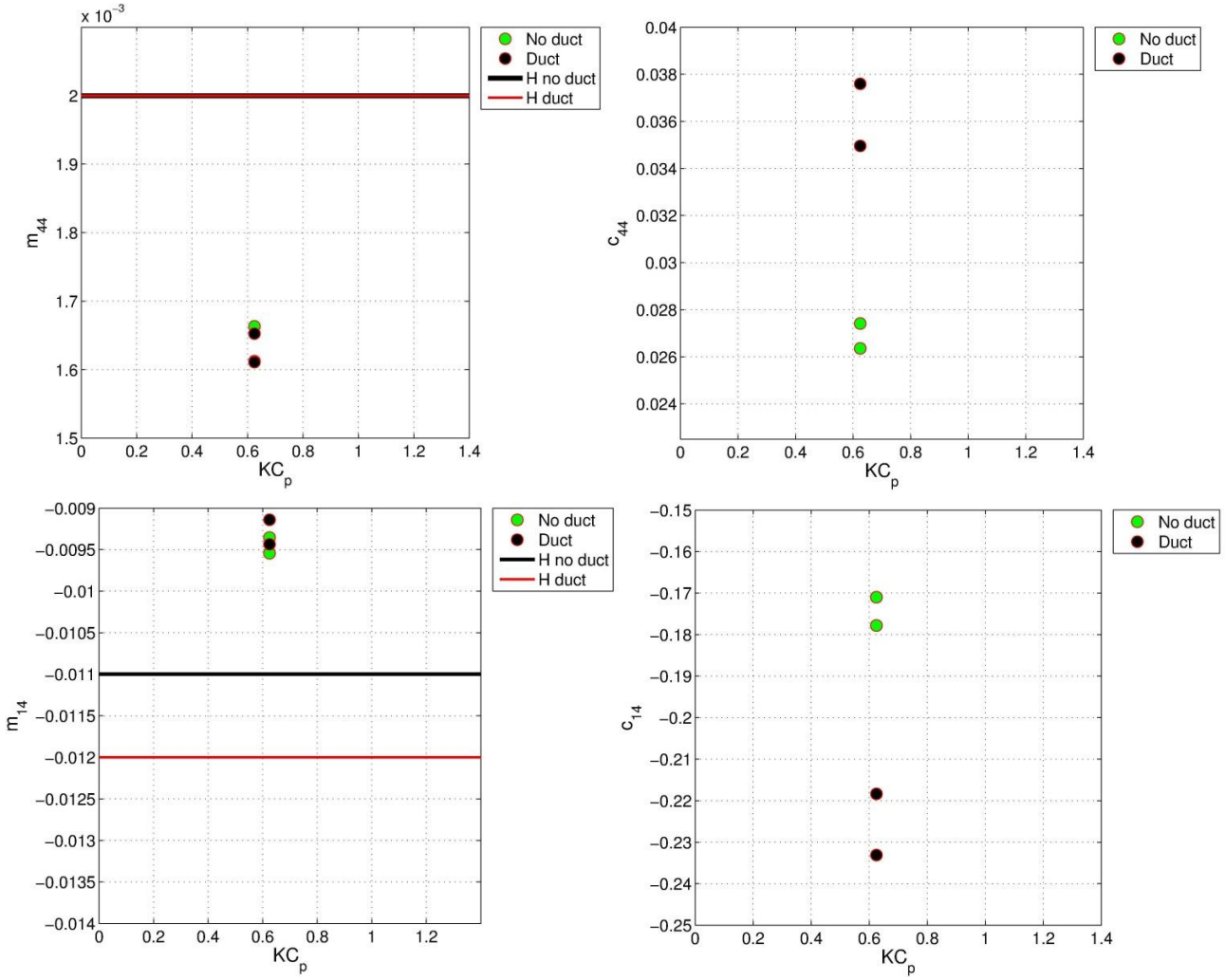

Figure 11. Computed force coefficients for cases f_e=22.5 Hz, x_{4a}=1.0 deg and f_e =22.5 Hz, x_{4a}=5.0 deg at J=0.8 for both the ducted and open propeller cases. 'H' stands for the potential flow computations by Hutchison (2013).

Table VII. Force coefficients of the oblique flow cases.

Flow angle [deg]	K_{T1}	m_{11}	c_{11}	m_{41}	c_{41}
0	0.226	0.0597	0.649	-0.00934	-0.0805
5	0.228	0.0504	0.695	-0.00738	-0.0924
10	0.234	0.0499	0.690	-0.00732	-0.0922
20	0.261	0.0502	0.695	-0.00735	-0.0902

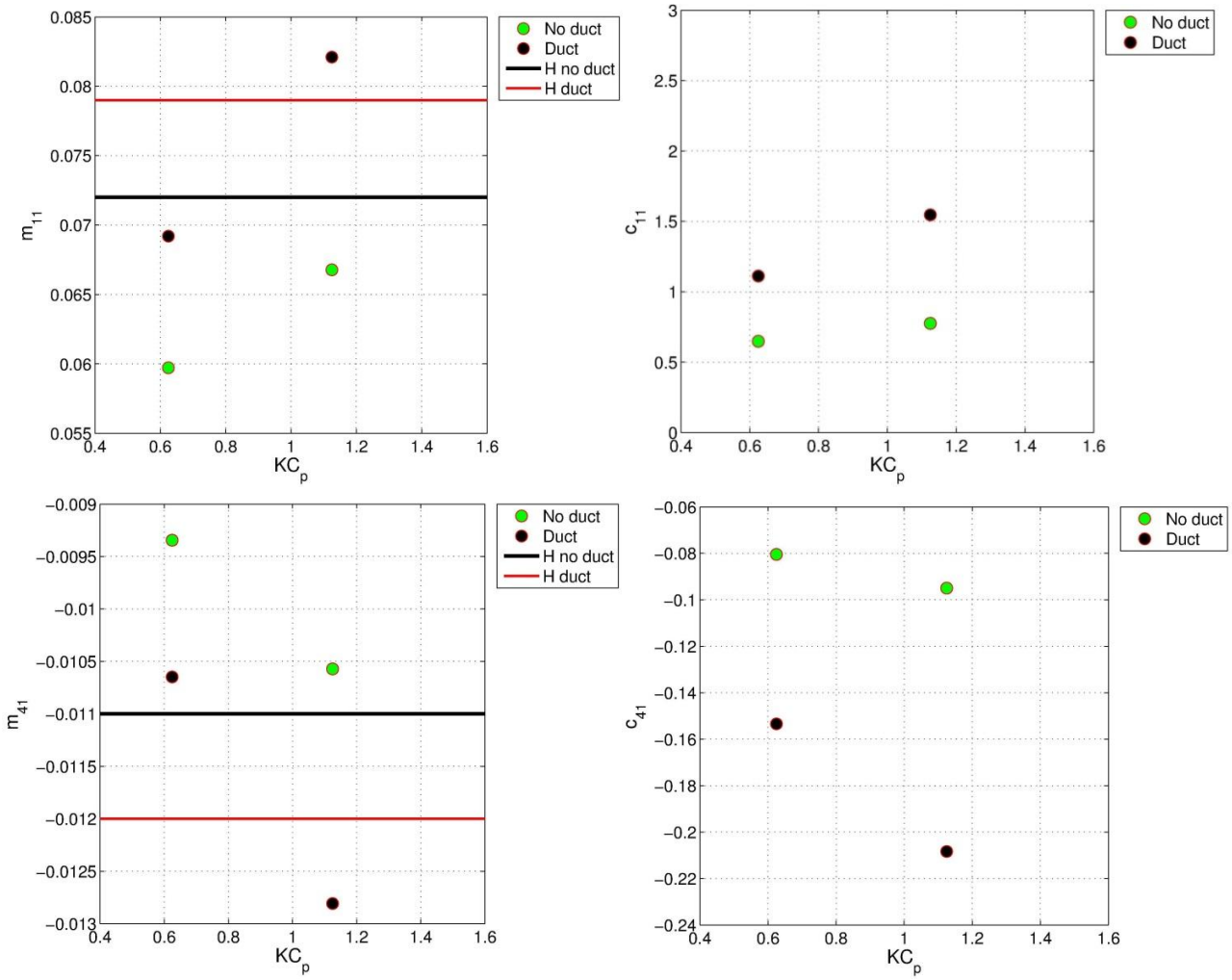

Figure 12. Computed forces as a function of time [s] for cases f_e=22.5 Hz, $\acute{x}_{1a}$=6.37 m/s (top) and f_e =40.5 Hz, $\dot{x}_{1a}$ =23.9 m/s (bottom) at J=0.8 for both the ducted and open propeller cases. 'H' stands for the potential flow computations by Hutchison (2013).

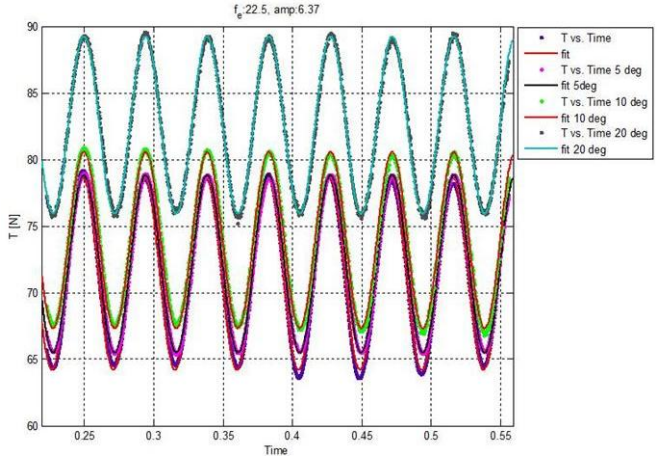

Figure 13. Computed thrust forces as a function of time [s] for the oblique cases.

REFERENCES

Carlton, J.S. (2007) "Marine Propellers and Propulsion," 2nd edition. Butterworth-Heinemann ISBN: 978-0-7506-8150-6

Gaschler, M. and Abdel-Maksoud, M. 2014. "Computation of Hydrodynamic Mass and Damping Coefficients for a Cavitating Marine Propeller Flow Using a Panel Method". Journal of Fluids and Structures 49 (2014) 574–593

Ghassemi, H. and Yari, E. 2011. "The Added Mass Coefficient computation of sphere, ellipsoid and marine propellers using Boundary Element Method". Polish Maritime Research. 1(68) 2011 Vol 18; pp. 17-26 10.2478/v10012-011-0003-1

Hutchison, S., Steen, S., and Sanghani, A. (2013), "Numerical Investigation of Ducted Propeller Added Mass," Proceedings of the Third International Symposium on Marine Propulsors - smp13, 5-8 May 2013, Launceston, Tasmania, Australia

Koushan, K. (2006), "Dynamics of ventilated propeller blade loading on thrusters," Proceedings of WMTC2006 World Maritime Technology Conference, London.

Lie, L.I., Chuan-Jing, L.U. and Xuan, H. 2010, "Calculation of Added Mass of a Vehicle Running with Cavity," Journal of Hydrodynamics. 2010, 22(3):312-318 DOI: 10.1016/S1001-6058(09)60060-3

MacPherson, D.M., Puleo, V.R., Packard, M.B., 2007. "Estimation of Entrained Water Added Mass Properties for Vibration Analysis", SNAME New England Section.

Martio, J., Sánchez-Caja A.,·and Siikonen T., (2015). "Evaluation of Propeller Virtual Mass and Damping Coefficients by URANS Method," Fourth International Symposium on Marine Propulsors - smp15, Austin, Texas, USA, 06/2015

Matusiak, J., (1986). "Theoretical Solutions for some Particular Problems of Ship Hydrodynamics," VTT publication 68.

Miettinen, A., and T. Siikonen. "Application of pressure- and density-based methods for different flow speeds." International Journal for Numerical Methods in Fluids Vol 79 pp. 243-267 (2015).

Mishra, V.; Vengadesan, S.; Bhattacharyya, S.K.. (2011). "Translational Added Mass of Axisymmetric Underwater Vehicles with Forward Speed Using Computational Fluid Dynamics" Journal of Ship Research, Volume 55, Number 3.

Parsons and Vorus (1981) "Added Mass and Damping Estimates for Vibrating Propellers" Proceedings of the Propellers Symposium Transactions SNAME, Virginia Beach, Va, USA, 1981.

Parsons M.G. (1983), "Mode Coupling in Torsional and Longitudinal Shafting Vibration," Marine Technology, Vol. 20 no. 3.

Sánchez-Caja, A., Rautaheimo, P., Salminen, E., and Siikonen, T., "Computation of the Incompressible Viscous Flow around a Tractor Thruster Using a Sliding Mesh Technique," 7th International Conference in Numerical Ship Hydrodynamics, Nantes (France), 1999.

Schwanecke, H., "Gedanken zur Frage der hydrodynamisch erregten Schwingungen des Propellers und der Wellenleitung", Jahrbuch STG, 1963.

Takeuchi M., Osaki, E. and Kon, Y. (1983), "Studies on the Added Mass and Added Moment of Inertia of Propellers," Journal of Shimonoseki University of Fisheries.

Uhlman, J.S., Fine, N.E. and Kring, D.C. , (2001) "Calculation of the Added Mass and Damping Forces on Supercavitating Bodies," In: CAV 2001: Fourth International Symposium on Cavitation, June 20-23, 2001, California Institute of Technology, Pasadena, CA USA.

Vassilopoulos, L. and Triantafyllou, M. (1981), "Prediction of Propeller Hydrodynamic Coefficients Using Unsteady Lifting Surface Theory. Proceedings of the Propellers Symposium Transactions SNAME, Virginia Beach, Va, USA, 1981.